Plasmonics (2014) 9:1471–1480
DOI 10.1007/s11468-014-9766-4

Nonlinear Optical Properties of Large-Sized Gold Nanorods

Guangyin Liu · Haidong Deng · Guangcan Li · Lei Chen · Qiaofeng Dai · Sheng Lan · Shaolong Tie

Received: 4 April 2014 / Accepted: 6 August 2014 / Published online: 19 August 2014

Abstract The nonlinear optical properties of single gold nanorods (GNRs) with a large diameter of ~200 nm and a long length of ~800 nm were investigated by using a focused femtosecond (fs) laser light with tunable wavelength. While the linear and nonlinear optical properties of small-sized GNRs have been extensively studied, the nonlinear optical properties of large-sized GNRs and the effects of high-order surface plasmon resonances remain unexplored. Second harmonic generation (SHG) or/and two-photon-induced luminescence (TPL) were observed in the nonlinear response spectra, and their dependences on excitation wavelength and polarization were examined. The scattering and absorption spectra of the small- and large-sized GNRs were compared by using the discrete dipole approximation method. It was found that the extinction of large-sized GNRs is dominated by scattering rather than absorption, which is dominant in small-sized GNRs. In addition, it was revealed that the excitation wavelength-dependent SHG of a GNR is governed by the linear scattering of the GNR and the maximum SHG is achieved at the valley of the scattering spectrum. In comparison, the excitation wavelength dependence of TPL is determined by the absorption spectrum of the GNR. The polarization-dependent SHG of a GNR exhibits a strong dependence on the dimension of the GNR, and it may appear as bipolar distributions parallel or perpendicular to the long axis of the GNR or multipole distributions.

Keywords Gold nanorods · Surface plasmon resonances · Second harmonic generation · Two-photon-induced luminescence · Femtosecond laser light

G. Liu · G. Li · L. Chen · Q. Dai · S. Lan (✉)
Laboratory of Nanophotonic Functional Materials and Devices, School of Information and Optoelectronic Science and Engineering, South China Normal University, Guangzhou 510006, China
e-mail: slan@scnu.edu.cn

H. Deng
College of Science, South China Agricultural University, Guangzhou 510642, China

S. Tie
School of Chemistry and Environment, South China Normal University, Guangzhou 510006, China

Introduction

Surface plasmon polaritons (SPPs) are collective oscillations of free electrons in metals [1]. Localized SPPs or surface plasmon resonances (SPRs), which are generally present in metallic micro- or nanoparticles (NPs) [2], have attracted great interest in the past decade because of the significant enhancement in electric field induced by SPRs [3]. A typical example is surface-enhanced Raman scattering which makes it possible for detecting the Raman signal of single molecules [4–6]. Among various metallic NPs, gold nanorods (GNRs) have been the focus of many studies due to the chemical stability of gold and particularly the existence of longitudinal SPRs (LSPRs) that give rise to extremely large enhancement in electric field [7, 8]. Other important features of the LSPRs of GNRs include their strong dependences on the aspect ratios of GNRs, the polarization of the excitation light, and the refractive index of the surrounding environment [9–11]. In practice, these features have been successfully exploited to fabricate optical functional materials and devices such as five-dimensional optical storage media [12–14] and various sensors [15–18].

So far, most studies in this field focus on the physical properties of small-sized GNRs, including synthesis method [19–21], self-alignment [22], electric and optical manipulations [23–26], linear [27, 28] and nonlinear optical properties [29–31], and transient optical properties [32], etc. The length

of such small-sized GNRs is usually smaller than 100 nm. Due to their small sizes, the extinction of such GNRs is generally dominated by absorption and scattering is almost negligible. Our recent study reveals that the nonlinear optical responses of such GNRs, which are governed by two-photon-induced luminescence (TPL), are closely related to the dominant role of absorption in such GNRs [33].

In contrast to the intensive and extensive studies on small GNRs, less attention has been paid to large GNRs whose length is much larger than 100 nm. Although the practical applications of such large GNRs remain unexplored, some initial studies on them have been carried out. For example, Payne et al. synthesized large GNRs with lengths longer than 1.0 μm and observed high-order SPRs in the extinction spectra of the GNRs [34]. For the characterization of nonlinear optical properties, Okamoto and Imura employed near field excitation to investigate the TPL from large GNRs and suggested consecutive absorption of two photons in the GNRs as the physical mechanism for TPL [35].

In this article, we present a systematic study on the nonlinear optical properties of single large-sized GNRs with a diameter of ~200 nm and an aspect ratio (AR) of ~4.0 and demonstrate the effects of high-order SPRs. It is found that the nonlinear optical responses of such GNRs are still governed by the high-order SPRs. Consequently, the excitation wavelength-dependent SHG and TPL are determined by the scattering and absorption spectra of GNRs. In addition, the polarization-dependent SHG of a GNR exhibits a strong dependence on the dimension of the GNR. Therefore, the nonlinear optical responses of large GNRs are more complicated than those of small GNRs.

Description of Sample, Numerical Method, and Experimental Setup

Sample Description

The large-sized GNRs used in our experiments were purchased from Nanoparts (Salt Lake City, UT). The sizes of GNRs were found to scatter in a large range. We analyzed the morphologies of a large number of GNRs by using scanning electron microscopy (SEM), and the images for some typical GNRs are shown in Fig. 1.

In Fig. 1, we can see GNRs with different diameters ranging from 200 to 280 nm and different aspect ratios ranging from 3.27 to 5.18. Most GNRs have cigar-like shapes composed of a cylinder and two hemispheres (see Fig. 1b, c, e, and h). In contrast, some GNRs have irregular shapes (see Fig. 1a, d, and g) or even have imperfections (see Fig. 1f). It is expected that the dimensions and morphologies of GNRs play an important role in determining their nonlinear optical responses, as demonstrated in the following.

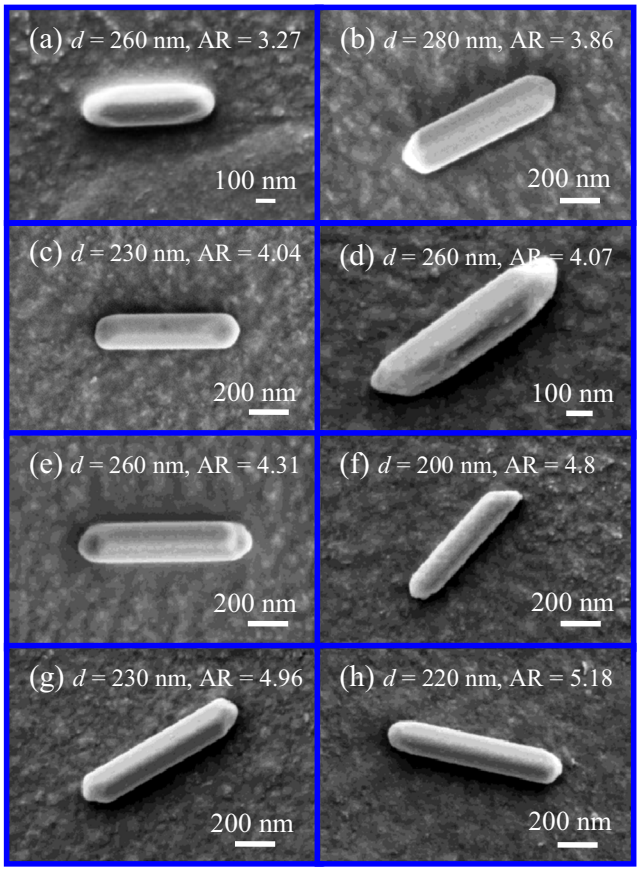

Fig. 1 SEM images of large-sized GNRs with different diameters and aspect ratios

Numerical Method and Experimental Setup

In order to understand the nonlinear optical responses of GNRs, we employed the discrete dipole approximation (DDA) method [36–38] to calculate the extinction, scattering, and absorption spectra of GNRs under different excitation conditions (different excitation wavelengths and excitation polarizations). The electric field distributions in GNRs were also simulated by using this method.

For the characterization of nonlinear optical properties, the GNRs used for measurements were uniformly distributed on a cover glass slide by dropping and drying the aqueous solution of GNRs on the glass slide. The femtosecond (fs) laser light delivered by a Ti:sapphire oscillator (Mira 900S, Coherent) with a pulse duration of 130 fs and a repetition rate of 76 MHz was focused on GNRs by using the objective lens (×100, NA=1.43) of an inverted microscope (Axio Observer A1, Zeiss). The excitation wavelength was tunable in the wavelength range of 760–810 nm. The emitted nonlinear signals such as SHG and TPL were collected by using the same objective lens and directed into a spectrometer (SR-500i-B1, Andor) equipped with a charge-coupled device (CCD) (DU970N, Andor) for analysis. Another CCD (DU897,

Andor) connected to the microscope was used to examine the orientations of GNRs and the location of the excitation spot. A combination of a half-wavelength plate and a quarter-wavelength one was employed to adjust the polarization of the fs laser light on the plane of the glass slide. In all measurements, we carefully compared the nonlinear optical signals detected at the place with GNRs with that without GNRs (bare glass slide). Under the maximum excitation densities we used in the experiments, we did not observe any obvious nonlinear optical signal from the glass slide. The vertical resolution of the microscope is 200 nm, and the maximum nonlinear signals were found when the laser light was focused slightly above the glass slide where GNRs were located.

Results and Discussion

Comparison of Linear Optical Properties Between Small-Sized and Large-Sized GNRs

As mentioned at the beginning, the linear optical properties of small-sized GNRs with diameters ranging from several to several tens nanometers have been extensively studied both theoretically and experimentally [39]. Basically, one can find two SPRs, which correspond to the transverse and longitudinal oscillations of electrons, respectively, in the extinction spectra of small-sized GNRs. While the transverse SPRs are not so sensitive to the dimensions of GNRs, the LSPRs exhibit a strong dependence on the aspect ratio of GNRs and their wavelengths are shifted to longer wavelengths with increasing aspect ratio. In general, the LSPR of a small-sized GNR appears in the near-infrared region and its wavelength is much larger than the dimension of the GNR. As a result, the scattering of the GNR is quite small and the extinction of the GNR is governed by the absorption [9, 33]. The calculated electric field of the GNR reveals the existence of a large enhancement in the electric field intensity inside or near the GNR. For the purpose of comparison, we calculated the extinction, scattering, and absorption spectra of a small-sized GNR with a cigar-like shape in air, as shown in Fig. 2a. The diameter and length of the GNR were chosen to be 10 and 40 nm. The polarization of the incident light was set to be parallel to the long axis of the GNR, corresponding to a polarization angle of θ=0°. The extinction, scattering, and absorption of the GNR are represented by the extinction, scattering, and absorption efficiencies which are the corresponding cross sections divided by the effective cross section of the GNR. It can be seen that the LSPR of the GNR appears at ~665 nm with a line width (full width at the half maximum) of ~38 nm. It is thought that the narrow line width of the LSPR is responsible for the significant enhancement in electric field intensity. It is noticed that the absorption is much larger than the scattering, and nearly

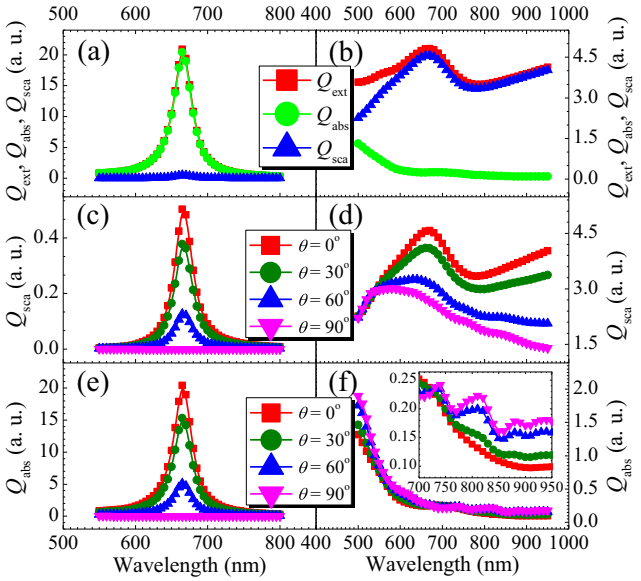

Fig. 2 Extinction, scattering, and absorption spectra of the small-sized (**a**) and large-sized (**b**) GNRs for a polarization angle of θ=0°. The evolutions of the scattering and absorption spectra with increasing polarization angle are presented in **c** and **e** for the small-sized GNR and in **d** and **f** for the large-sized GNR

98 % of the extinction comes from the absorption. When the polarization angle is increased, both the scattering and the absorption are reduced, as shown in Fig. 2c, e where the scattering and absorption efficiencies at different polarization angles of θ=0, 30, 60, and 90° are presented. However, it is noticed that the wavelength of the LSPR remains nearly unchanged.

Now, let us examine the linear optical properties of a large-sized GNR whose dimension is magnified by a factor of 20. The diameter and length of the GNR are chosen to be 200 and 800 nm, respectively. In Fig. 2b, we show the calculated extinction, scattering, and absorption spectra of the GNR for θ=0°. The spectra span from the visible to near-infrared spectral region in which the nonlinear optical properties of the GNR will be investigated. Different from the small-sized GNR whose extinction is governed by absorption, it is remarkable that the extinction of the large-sized GNR is dominated by scattering which is more than one order of magnitude larger than absorption. This is the major difference in the extinction spectra between the small-sized and large-sized GNRs. For comparison, the evolutions of the scattering and absorption spectra with increasing polarization angle are presented in Fig. 2d, f. In the scattering spectrum shown in Fig. 2d, one can see a resonant peak at ~670 nm for θ=0°. This peak is blue shifted to 660, 650, and 590 nm for θ=30, 60, and 90°. In addition, we observe a valley at ~790 nm for θ=0° and a valley at ~800 nm for θ=30°. In contrast, only a monotonic decrease of scattering is observed for θ=60 and 90° at the long-wavelength side of the scattering peak. It is also noticed that the resonant peaks in all cases appear to be

broad. This polarization dependence of scattering is completely different from what we observe in the small-sized GNR whose LSPR is independent on polarization angle. In Fig. 2f, the absorption for θ=0 and 30° exhibits a monotonic decrease in the wavelength range of 700–950 nm while that for θ=60 and 90° exhibits an oscillation with peaks and valleys in this wavelength region (see the inset in Fig. 2f).

Actually, the SPR shown in Fig. 2b is one of the high-order SPRs of the large-sized GNR. It can be easily identified in the extinction spectrum of the large-sized GNR over a wider spectral region, as shown in Fig. 3a. As compared to the low-order SPR peaking at ~2,100 nm, the high-order SPR appears to be much weaker. Limited by the fs laser source and the multiphoton absorption in gold, we can only investigate the effects of the high-order SPR on the nonlinear optical properties of large-sized GNRs. In Fig. 3b, c, we present the calculated electric field intensity distributions in the large-sized GNR at the low-order SPR (2,100 nm) for polarization angles of θ=0 and 90°. It can be seen later that the electric field intensity distribution appears to be different for the low- and high-order SPRs.

In Fig. 4a, b, we show the electric field intensity (E^2) distributions calculated for the small-sized GNR at the LSPR (665 nm) for θ=0 and 90°. It can be seen that the maximum enhancement factor in electric field intensity as large as ~10^4 is achieved in the GNR for θ=0°. For θ=90°, the electric field intensity is quite weak. For comparison, we present in Fig. 4c, d the electric field intensity distributions calculated for the large-sized GNR at the resonant peak of the scattering spectrum (~670 nm) for θ=0 and 90°. For θ=0°, it can be seen that the maximum enhancement factor in electric field

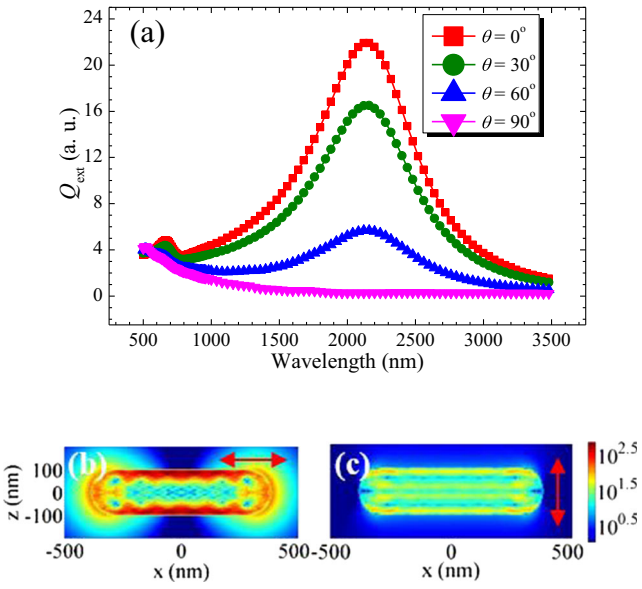

Fig. 3 **a** Extinction spectra of the large-sized GNR calculated for different polarization angles. The electric field distributions at the low-order SPR (2,100 nm) for polarization angles of θ=0 and 90° are presented in **b** and **c**

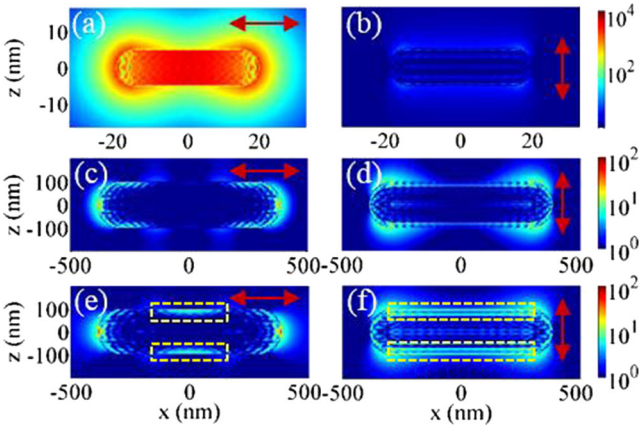

Fig. 4 Calculated electric field intensity distributions in the small-sized GNR for θ=0° (**a**) and θ=90° (**b**). **c** and **d** show the electric field intensity distributions for the large-sized GNR at the peak of the scattering spectrum for θ=0 and 90°. **e** and **f** show the calculated electric field intensity distributions at the valley of the scattering spectrum for θ=0 and 90°

intensity, which is estimated to be ~10^2, is reduced by more than two orders of magnitude as compared to that in the small-sized GNR. A detailed comparison of the electric field intensities and the absorption cross sections at different wavelengths reveals that the larger the absorption, the stronger is the electric field intensity. Although a significant reduction in the enhancement factor is observed for θ=0°, it is remarkable that a dramatic increase in the enhancement factor is found for θ=90°. Consequently, the electric field intensity in this case appears to be comparable to that obtained for θ=0°. This feature indicates that large-sized GNRs will exhibit nonlinear optical responses that are much different from those of small-sized GNRs. We also examined the electric field intensity distributions in the large-sized GNR at the valley of the scattering spectrum (~790 nm), as shown in Fig. 4e, f for θ=0 and 90°. The maximum enhancement factor in the electric field intensity is found to be similar to that observed at the peak of the scattering spectrum. A close inspection reveals, however, that the electric field intensity distributions are different in these two cases. While the electric field is concentrated at the two ends of the GNR in the former case, the electric field on the two sides becomes significant in the latter case, as indicated by the dashed boxes in Fig. 4e, f.

Excitation Wavelength-Dependent Nonlinear Optical Responses of Large-Sized GNRs

Having known the differences in SPRs between small-sized and large-sized GNRs, we examined the nonlinear optical response of a large-sized GNR, whose CCD image and scattering spectrum are shown in Fig. 5a, b, by focusing a fs laser beam on the GNR. The polarization of the fs laser light was chosen to be parallel to the long axis of the GNR, corresponding to θ=0°. The scattering spectrum shown in Fig. 5b was obtained by using dark-field microscopy. It will be shown

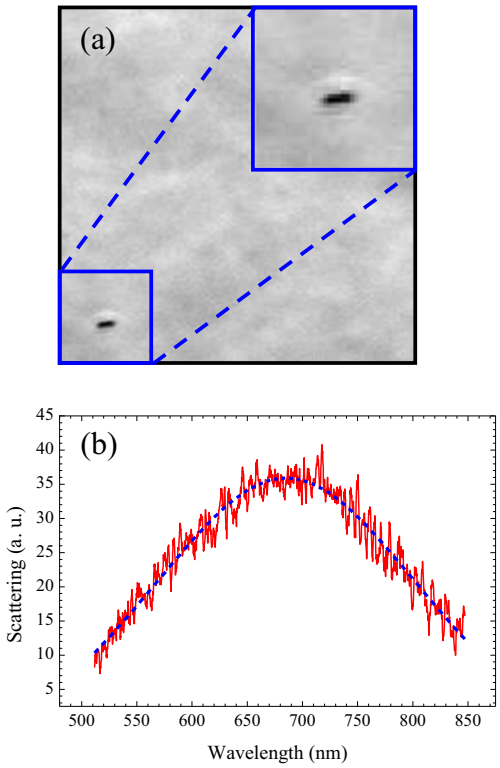

Fig. 5 CCD image (**a**) and scattering spectrum (**b**) of the GNR

later that the scattering peak depends not only on the aspect ratio of the GNR but also on its diameter. Based on the scattering peak which is located at ~670 nm, one can estimate the aspect ratio and diameter of the GNR, which is quite important for comparing the experimental observations with the simulations results. The GNR may have an aspect ratio of ~4.0 and a diameter of ~200 nm (see Fig. 9).

In order to see the effects of the high-order SPR on the nonlinear optical properties of large-sized GNRs, we measured the nonlinear response spectra of the GNR at different excitation wavelengths ranging from 780 to 810 nm, as shown in Fig. 6a. At 810 nm, the nonlinear response spectrum is dominated by strong SHG with negligible TPL. When the excitation wavelength is tuned to shorter wavelengths, it is found that the intensity of SHG increases with decreasing wavelength and reaches its maximum value at 795 nm. After that, the intensity of SHG begins to decrease with decreasing wavelength. Meanwhile, it is noticed that the intensity of TPL increases gradually at first and rapidly for wavelengths shorter than 785 nm. The dependence of SHG on excitation intensity was examined at 800 nm, and the result is plotted in a logarithmic coordinate, as shown in Fig. 6b. The fitting of the experimental data gives a slope of ~1.92, which is in good agreement with the second-order nature of SHG. This feature

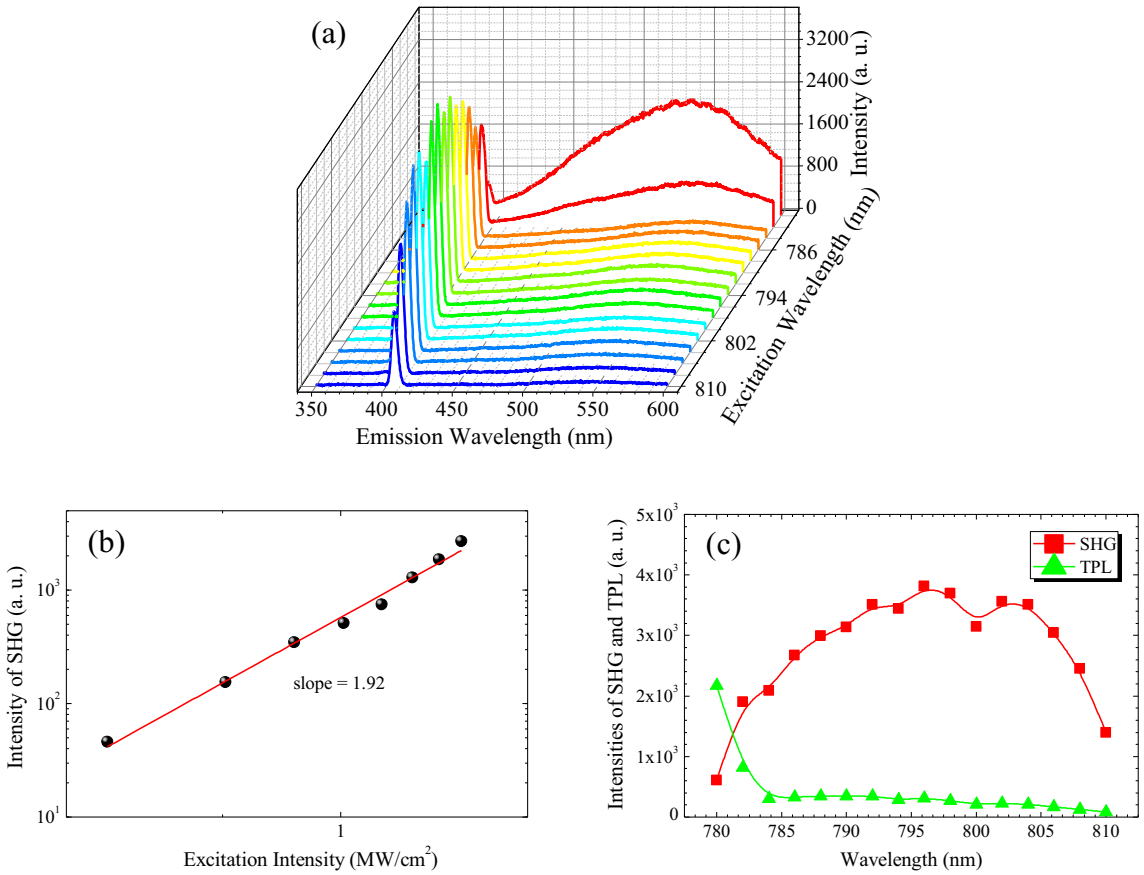

Fig. 6 **a** Evolution of the nonlinear response spectrum of the GNR with decreasing excitation wavelength. **b** Excitation intensity-dependent SHG measured at 800 nm. **c** Dependences of the nonlinear optical signals (SHG/TPL) on excitation wavelength measured for the GNR

is completely different from what we observed in small-sized GNRs whose nonlinear response spectra are generally governed by TPL [33]. The dependences of the intensities of SHG and TPL on excitation wavelength are summarized in Fig. 6c. One can see that a maximum of SHG appears at 795 nm while a rapid increase in TPL occurs at ~780 nm. The intensity of SHG at 795 nm is about eight times of that at 780 nm. On the other hand, the intensity of TPL at 780 nm is one order of magnitude larger than that at 810 nm.

In order to find out the correlation between the high-order SPR and the nonlinear optical responses of large-sized GNRs, we measured another GNR whose CCD image is shown in Fig. 7a. The diameter and aspect ratio of the GNR are quite similar to those shown in Fig. 5a, but its long axis is almost along the vertical direction. The scattering peak was also observed at ~670 nm, confirming the similar diameter and aspect ratio of the GNR with that shown in Fig. 5a. Similarly, we measured the nonlinear response spectra of the GNR at

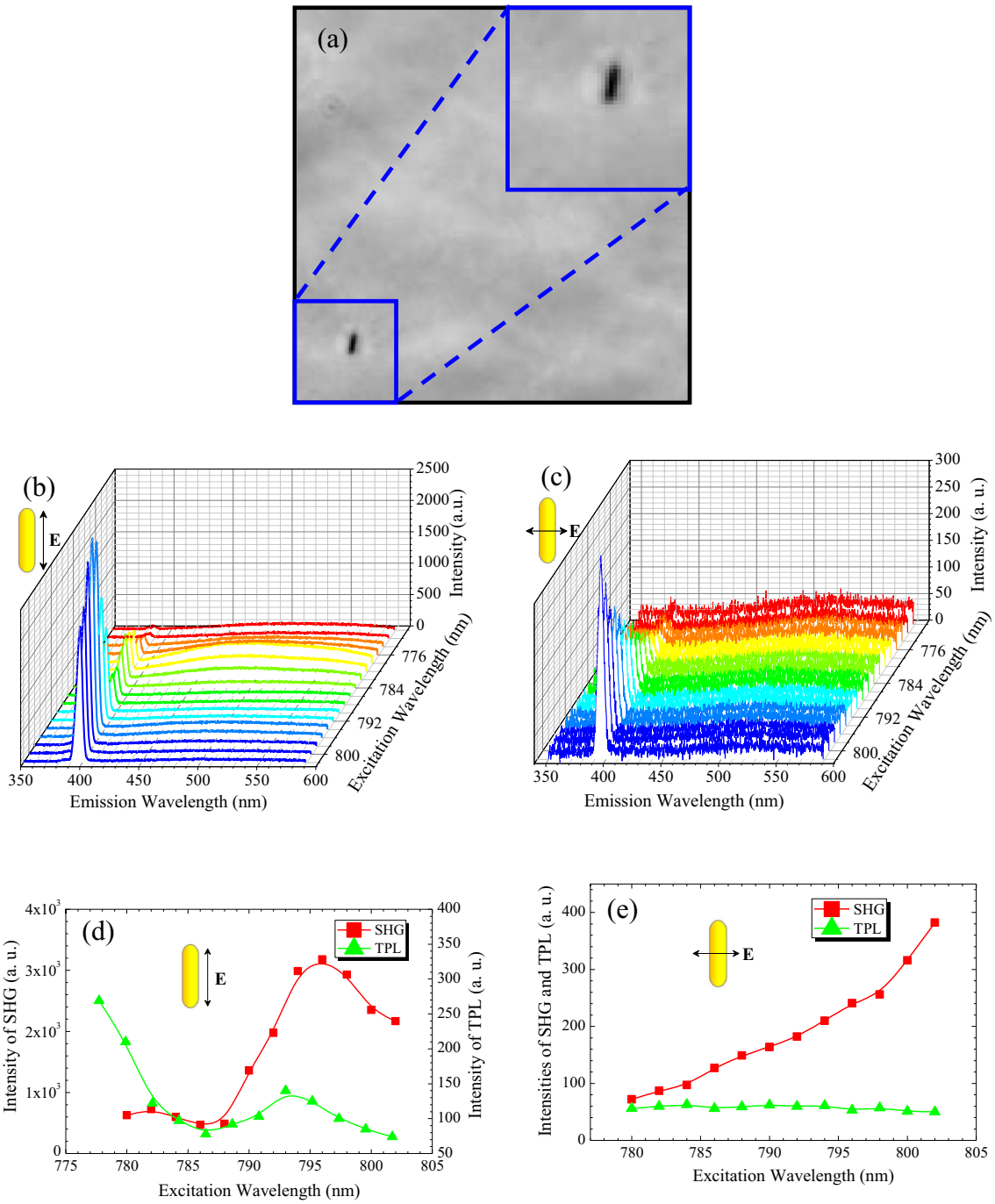

Fig. 7 **a** CCD image of the GNR. **b** and **c** Excitation wavelength-dependent nonlinear response spectra of the GNR measured for polarization angles of θ=0 and 90°. **d** and **e** Excitation wavelength-dependent nonlinear optical signals (SHG/TPL) of the GNR for polarization angles of θ=0 and 90°

different excitation wavelengths. The results for two polarization angles of θ=0 and 90° are presented in Fig. 7b, c. The dependences of the nonlinear optical signals (SHG/TPL) on excitation wavelength are summarized in Fig. 7d, e for θ=0 and 90°, respectively. In Fig. 7d, we can see that the intensity of SHG is about one order of magnitude larger than that of TPL. For the excitation wavelength-dependent SHG, one can see a maximum at ~796 nm. The maximum for the TPL is observed at 778 nm. For θ=90°, the nonlinear optical response appears to be completely different, as shown in Fig. 7e. In this case, a monotonic increase in SHG is observed with increasing excitation wavelength. However, the absolute intensity of SHG is much weaker than that observed for θ=0°. In sharp contrast, the intensity of TPL appears to be quite weak and it is not sensitive to excitation wavelength. The physical mechanism responsible for the different nonlinear optical responses will be discussed later.

Polarization-Dependent SHG and TPL in Large-Sized GNRs

In the last section, we have shown that large-sized GNRs exhibit nonlinear optical responses that are completely different from those of small-sized GNRs. In addition, it has been shown that the nonlinear optical response of a large-sized GNR depends strongly on the polarization of the excitation light with respect to the long axis of the GNR. In order to gain a deep insight into the dependence of nonlinear optical response on excitation polarization, we examined the excitation polarization-dependent nonlinear optical response for a large number of GNRs. It is found that for most GNRs, the nonlinear optical responses are dominated by SHG with negligible TPL at an excitation wavelength of 800 nm. This is completely different from the nonlinear optical responses of small-sized GNRs which are governed by TPL. For small-sized GNRs, a $\cos^4\theta$ dependence of TPL on polarization angle θ is generally observed regardless of the diameters and aspect ratios of GNRs [29]. This characteristic is determined by the physical properties of small-sized GNRs shown in Fig. 2a, c, and e which are not sensitive to the size and shape of GNRs.

For the large-sized GNRs studied in this paper, it is found that their nonlinear optical properties exhibit strong dependences on the size, shape, and even imperfections of GNRs. In Fig. 8, we present three typical polarization dependences of SHG observed in large-sized GNRs. The CCD images for the corresponding GNRs are also provided to show the morphologies and orientations of the GNRs. In Fig. 8a, the polarization-dependent SHG exhibits a bipolar distribution parallel to the long axis of the GNR, similar to that observed in the polarization-dependent TPL of a small-sized GNR. When we try to fit the experimental data with a function of $\cos^4\theta$, however, a relatively large discrepancy is observed. It is found that the discrepancy occurs mainly in the direction perpendicular to the long axis of the GNR (θ=90°) for which there exists a large enhancement in electric field intensity, as can be seen in Fig. 4d, f. Consequently, the nonlinear optical response does not disappear in this direction, leading to the deviation of the experimental data from the function of $\cos^4\theta$.

Apart from the bipolar distribution of SHG parallel to the long axis of the GNR observed in Fig. 8a, we also found some GNRs which exhibit a bipolar distribution of SHG perpendicular to the long axis of the GNR, as shown Fig. 8b. In this case, it implies that the nonlinear optical response of the GNR is stronger in the direction of θ=90° than that in the direction of θ=0°. This feature is not observed in small-sized GNRs, and it is closely related to the physical properties of large-sized GNRs described above. The experimental data shown in Fig. 8a, b can be better described by a function of $\cos^4\theta + C$, where C is a constant. More surprisingly, we observed in rare cases a quadrupole distribution in the excitation polarization dependence of SHG which can be fitted by $\sin^2\theta + \cos^2\theta + C$, as shown in Fig. 8c. In this case, the strongest SHG is observed in a direction between θ=0° and θ=90°. It further indicates that the nonlinear optical responses of large-sized GNRs depend strongly on the size and morphology of GNRs.

Relationship Between Linear and Nonlinear Optical Properties

Basically, the nonlinear optical response of a large-sized GNR is determined by the enhancement in electric field intensity induced by the SPRs of the GNR. Therefore, there should be a correlation between the nonlinear optical response and the linear optical properties of the GNR. Since the linear optical properties of a GNR depend not only on the diameter but also on the aspect ratio of the GNR, we show the evolution of extinction spectrum with increasing diameter for a fixed aspect ratio of AR=4.0 in Fig. 9a and the evolution of extinction spectrum with increasing aspect ratio for a fixed diameter of d=200 nm in Fig. 9b. The polarization angle is chosen to be θ=0°. In Fig. 9a, one can see a peak and a valley in the spectral region of 550–950 nm. With increasing diameter, a redshift of both the peak and the valley is observed. Similar evolution of the spectrum is found with increasing aspect ratio when the diameter is fixed at 200 nm, as shown in Fig. 9b. Since the extinction is dominated by scattering, one can refer that the GNRs shown in Figs. 5a and 7a have a diameter of ~200 nm and an aspect ratio of ~4.0 because their scattering peaks appear at ~670 nm. In this case, the scattering valley appears at 790 nm where the maximum of SHG is observed, as shown Figs. 6c and 7d. It implies that the SHG in large-sized GNRs is inversely proportional to the scattering. This conclusion is supported by the nonlinear optical response in the direction of θ=90° which shows a monotonic increase in SHG with increasing excitation wavelength, as shown in Fig. 7e. The evolutions of extinction spectrum calculated for θ=90° are

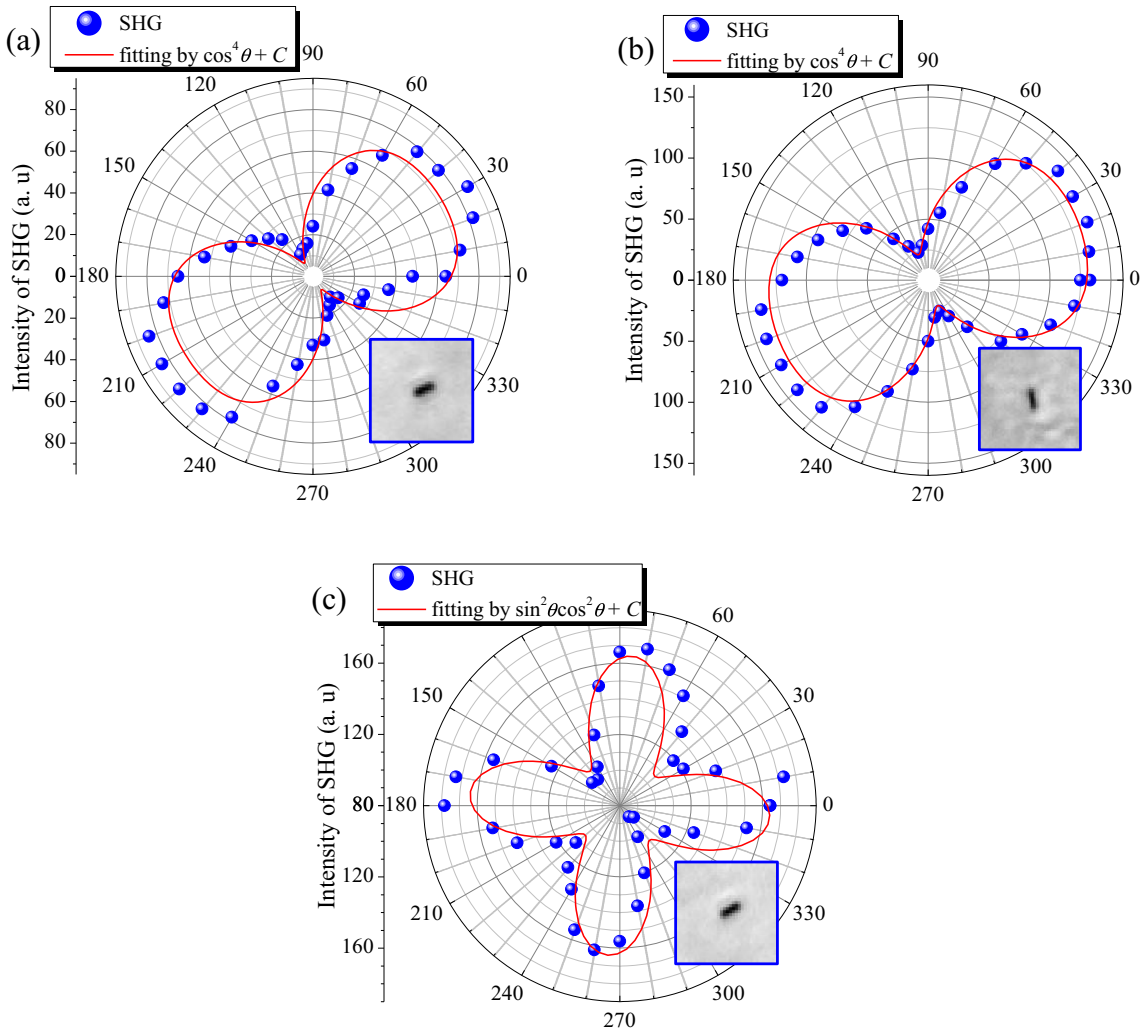

Fig. 8 **a** Polarization-dependent SHG showing a bipolar distribution of SHG parallel to the long axis of the GNR. **b** Polarization-dependent SHG showing a bipolar distribution of SHG perpendicular to the long axis of the GNR. **c** Polarization-dependent SHG showing a quadrupole distribution. The CCD images of the GNRs showing their morphologies and orientations are given in the *insets*

shown in Fig. 9c, d. In both cases, one can see a monotonic decrease of scattering with increasing wavelength.

The inversely proportional relationship between the scattering and the SHG can be understood from two aspects. In one hand, the energy of the excitation light has only two output channels if the TPL can be neglected. They are linear scattering and SHG which can be considered as nonlinear scattering process. If the linear scattering is strong, then the SHG is weak. On the other hand, gold is a material with centrosymmetry and the SHG in a GNR mainly comes from the surface material where the symmetry is broken [40, 41]. The contribution of bulk material to the SHG is quite small. Therefore, the concentration of electric field at the surface will facilitate SHG [42, 43]. As shown in Fig. 4e, f, the electric field is mainly concentrated at the two ends of the GNR at the wavelength corresponding to the scattering peak. In contrast, the electric field on the two sides of the GNR becomes

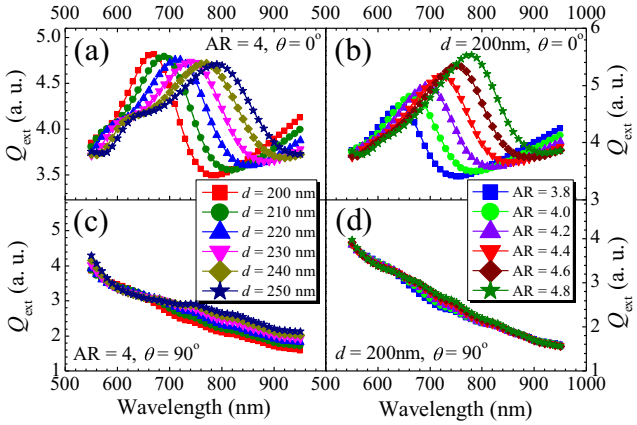

Fig. 9 Evolution of the extinction spectrum of a GNR with a fixed aspect ratio of AR=4.0 with an increasing diameter of the GNR for polarization angles of θ=0° (**a**) and θ=90° (**c**). The evolutions of the extinction spectrum of a GNR with a fixed diameter of d=200 nm with increasing aspect ratio are shown in **b** and **d** for θ=0° and θ=90°, respectively

significant when the wavelength is chosen at the scattering valley, as indicated by the dashed boxes in Fig. 4e, f. Consequently, an increase in SHG is expected at the scattering valley.

Having established the relationship between the SHG and the linear scattering, let us see whether there is a relationship between the linear absorption and the nonlinear absorption which is reflected in the TPL of the GNR. Basically, the linear absorption of a GNR is proportional to the integration of electric field intensity (E^2) over the GNR. It has been demonstrated that the nonlinear absorption such as the two-photon absorption considered here is determined by the integration of E^4 over the GNR [17]. Thus, it is expected that the nonlinear absorption exhibits a wavelength dependence similar to that of the linear absorption but with much more rapid change. From the absorption spectrum shown in Fig. 2d, one can see an increase in the absorption with decreasing wavelength. Accordingly, we observed a sharp increase in the TPL at shorter excitation wavelengths, as shown in Figs. 6c and 7e.

It is known that the GNRs shown in Figs. 6 and 7 have scattering peaks at ~670 nm and scattering valleys at ~790 nm. In this case, the SHG measured at 800 nm is stronger for θ=0° than that for θ=90°. As can be seen in Fig. 9a, b, the scattering peak can be shifted to ~800 nm if the diameter of the GNR is increased to ~250 nm (for AR= 4.0) or the aspect ratio of the GNR is increased to 4.8 (for d= 200 nm). For GNRs with such dimensions, a weak SHG is expected for θ=0°. For θ=90°, the increase in scattering is not large, so is the reduction in SHG. Therefore, it is expected that the SHG for θ=90° may exceed that for θ=0°, leading to a bipolar distribution of SHG perpendicular to the long axis of the GNR. This feature indicates that for large-sized GNRs, the strongest SHG may not appear at θ=0°. If the strongest SHG occurs at an angle in between 0 and 90°, then a quadrupole distribution of SHG will be observed, as shown in Fig. 8c.

Conclusion

In summary, we have investigated numerically and experimentally the effects of high-order SPRs on the nonlinear optical properties of large-sized GNRs. It is found that the extinction spectra of large-sized GNRs are dominated by scattering rather than absorption which governs the extinction spectra of small-sized GNRs. In addition, the enhancement factor in electric field intensity is reduced by two orders of magnitude for the longitudinal excitation while it is increased by two orders of magnitude for the transverse excitation as compared to that in small-sized GNRs. Different from small-sized GNRs whose nonlinear optical responses are governed by TPL, the nonlinear optical responses of large-sized GNRs are dominated by SHG. It is found that the wavelength- and polarization-dependent SHG exhibits strong dependences on the diameter and aspect ratio of GNRs, giving rise to bipolar SHG distributions parallel and perpendicular to the long axis of the GNR and even quadrupole distribution. The dependence of SHG on excitation polarization cannot be fitted with a function of $\cos^4\theta$. A correlation between the scattering spectrum and the wavelength dependence of SHG has been established, and it is revealed that SHG is reversely proportional to linear scattering. Furthermore, it is found that TPL exhibits wavelength dependence similar to that of linear absorption but with much more rapid change. The understanding of the nonlinear optical responses of large-sized GNRs will be helpful for exploring their applications in photonic functional materials and devices.

Acknowledgments The authors acknowledge the financial support from the National Natural Science Foundation of China (Grant Nos. 51171066 and 11374109), the Ministry of Education of China (Grant No. 20114407110002), and the project for high-level professionals in the universities of Guangdong province, China.

References

1. Raether H (1988) Surface plasmons on smooth and rough surfaces and on gratings. Springer, Berlin
2. Prasad PN (2004) Nanophotonics. John Wiley & Sons, New York
3. Brongersma ML, Kik PG (2007) Surface plasmon nanophotonics. Springer, Netherlands
4. Nie S, Emory SR (1997) Probing single molecules and single nanoparticles by surface-enhanced Raman scattering. Science 275:1102–1106
5. Qian X, Peng X, Ansari DO, Yin-Goen Q, Chen GZ, Shin DM, Yang L, Young AN, Wang MD, Nie S (2008) In vivo tumor targeting and spectroscopic detection with surface-enhanced Raman nanoparticle tags. Nat Biotechnol 26:83–90
6. Huang X, El-Sayed IH, Qian W, El-Sayed MA (2007) Cancer cells assemble and align gold nanorods conjugated to antibodies to produce highly enhanced, sharp, and polarized surface raman spectra: a potential cancer diagnostic marker. Nano Lett 7:1591–1597
7. Link S, El-Sayed MA (1999) Spectral properties and relaxation dynamics of surface plasmon electronic oscillations in gold and silver nanodots and nanorods. J Phys Chem B 103:8410–8426
8. Canfield BK, Husu H, Laukkanen J, Bai B, Kuittinen M, Turunen J, Kauranen M (2007) Local field asymmetry drives second-harmonic generation in noncentrosymmetric nanodimers. Nano Lett 7:1251–1255
9. Link S, Mohamed MB, El-Sayed MA (1999) Simulation of the optical absorption spectra of gold nanorods as a function of their aspect ratio and the effect of the medium dielectric constant. J Phys Chem B 103:3073–3077
10. Ming T, Zhao L, Yang Z, Chen H, Sun L, Wang J, Yan C (2009) Strong polarization dependence of plasmon-enhanced fluorescence on single gold nanorods. Nano Lett 9:3896–3903
11. Kelly KL, Coronado E, Zhao LL, Schatz GC (2003) The optical properties of metal nanoparticles: the influence of size, shape, and dielectric environment. J Phys Chem B 107:668–677
12. Chon JWM, Bullen C, Zijlstra P, Gu M (2007) Spectral encoding on gold nanorods doped in a silica sol–gel matrix and its application to high-density optical data storage. Adv Funct Mater 17:875–880

13. Zijlstra P, Chon JWM, Gu M (2009) Five-dimensional optical recording mediated by surface plasmons in gold nanorods. Nature 459: 410–413
14. Li X, Lan TH, Tien CH, Gu M (2012) Three-dimensional orientation-unlimited polarization encryption by a single optically configured vectorial beam. Nat Commun 3:998
15. Zijlstra P, Paulo PMR, Orrit M (2012) Optical detection of single non-absorbing molecules using the surface plasmon resonance of a gold nanorod. Nat Nanotechnol 7:379–382
16. Shao L, Fang C, Chen H, Man YC, Wang J, Lin HQ (2012) Distinct plasmonic manifestation on gold nanorods induced by the spatial perturbation of small gold nanospheres. Nano Lett 12:1424–1430
17. Chen L, Li GY, Liu GC, Dai QF, Lan S, Tie SL, Deng HD (2013) Sensing the moving direction, position, size, and material type of nanoparticles with the two-photon-induced luminescence of a single gold nanorod. J Phys Chem C 117:20146–201453
18. Sönnichsen C, Alivisatos AP (2005) Gold nanorods as novel nonbleaching plasmon-based orientation sensors for polarized single-particle microscopy. Nano Lett 5:301–304
19. Sau TK, Murphy CJ (2004) Seeded high yield synthesis of short Au nanorods in aqueous solution. Langmuir 20:6414–6420
20. Nikoobakht B, El-Sayed MA (2003) Preparation and growth mechanism of gold nanorods (NRs) using seed-mediated growth method. Chem Mater 15:1957–1962
21. Grzelczak M, Pérez-Juste J, Mulvaney P, Liz-Marzán LM (2008) Shape control in gold nanoparticle synthesis. Chem Soc Rev 37: 1783–1791
22. Khanal BP, Zubarev ER (2007) Rings of nanorods. Angew Chem Ed 46:2195–2198
23. Van der Zande BMI, Koper GJM, Lekkerkerker HNW (1999) Alignment of rod-shaped gold particles by electric fields. J Phys Chem B 103:5754–5760
24. Khatua S, Chang W, Swanglap P, Olson J, Link S (2011) Active modulation of nanorod plasmons. Nano Lett 11:3797–3802
25. Pelton M, Liu M, Kim HY, Smith G, Guyot-Sionnest P, Scherer NF (2006) Optical trapping and alignment of single gold nanorods by using plasmon resonances. Opt Lett 31:2075–2077
26. Zins I, Schubert O, Sönnichsen C, Oddershede LB (2008) Quantitative optical trapping of single gold nanorods. Nano Lett 8: 2998–3003
27. Mohamed MB, Volkov V, Link S, El-Sayed MA (2000) The 'lightning' gold nanorods: fluorescence enhancement of over a million compared to the gold metal. Chem Phys Lett 317:517–523
28. Eustis S, El-Sayed MA (2005) Aspect ratio dependence of the enhanced fluorescence intensity of gold nanorods: experimental and simulation study. J Phys Chem B 109:16350–16356
29. Wang H, Huff TB, Zweifel DA, He W, Low PS, Wei A, Cheng J (2005) In vitro and in vivo two-photon luminescence imaging of single gold nanorods. Proc Natl Acad Sci U S A 102:15752–15756
30. Hubert C, Billot L, Adam PM, Bachelot R, Royer P, Grand J, Gindre D, Dorkenoo KD, Ford A (2007) Role of surface plasmon in second harmonic generation from gold nanorods. Appl Phys Lett 90: 181105–181107
31. Butet J, Duboisset J, Bachelier G, Russier-Antoine I, Benichou E, Jonin C, Brevet P (2010) Optical second harmonic generation of single metallic nanoparticles embedded in a homogeneous medium. Nano Lett 10:1717–1721
32. Link S, Burda C, Mohamed MB, Nikoobakht B, El-Sayed MA (2000) Femtosecond transient absorption dynamics of colloidal gold nanorods: shape independence of the electron-phonon relaxation time. Phys Rev B 61:6066–6090
33. Deng HD, Li GC, Dai QF, Ouyang M, Lan S, Trofimov VA, Lysak TM (2013) Size dependent competition between second harmonic generation and two-photon luminescence observed in gold nanoparticles. Nanotechnology 24:075201
34. Payne EK, Shuford KL, Park S, Schatz GC, Mirkin CA (2006) Multipole plasmon resonances in gold nanorods. J Phys Chem B 110:2150–2154
35. Okamoto H, Imura K (2009) Near-field optical imaging of enhanced electric fields and plasmon waves in metal nanostructures. Prog Surf Sci 84:199–229
36. Yurkin MA, Maltsev VP, Hoekstra AG (2007) The discrete dipole approximation: an overview and recent developments. J Quant Spectrosc Radiat Transf 106:558–589
37. Draine BT, Flatau PJ (2009) User guide to the giscrete dipole approximation code, DDSCAT 7.0. http://arxiv.org/abs/0809.0337
38. The information on the refractive indices of materials are available on website http://refractiveindex.info/
39. Jain PK, Lee KS, El-Sayed IH, El-Sayed MA (2006) Calculated absorption and scattering properties of gold nanoparticles of different size, shape, and composition: applications in biological imaging and biomedicine. J Phys Chem B 110:7238–7248
40. Dadap JI, Shan J, Heinz TF (2004) Theory of optical second-harmonic generation from a sphere of centrosymmetric material: small-particle limit. J Opt Soc Am B 21:1328–1347
41. Dadap JI, Shan J, Eisenthal KB, Heinz TF (1999) Second-harmonic rayleigh scattering from a sphere of centrosymmetric material. Phys Rev Lett 83:4045–4048
42. Bachelier G, Butet J, Russier-Antoine I, Jonin C, Benichou E, Brevet PF (2010) Origin of optical second-harmonic generation in spherical gold nanoparticles: local surface and nonlocal bulk contributions. Phys Rev B 82:235403
43. Bachelier G, Russier-Antoine I, Benichou E, Jonin C, Brevet P (2008) Multipolar second-harmonic generation in noble metal nanoparticles. J Opt Soc Am B 25:955–960